temperature.[21] Finally, the chemical reactivity of dimethylamino radical with NO, $NO_2$ and dimethylnitramine is currently under investigation with the VLPR (very low pressure reactor) technique in order to obtain their rate constants and establish their reaction pathways.

## Conclusions

The infrared multiphoton dissociation of dimethylnitramine has been found to occur through scission of the weak N-$NO_2$ bond. The steady-state rate of decomposition has been estimated at various laser intensities and the average degree of laser excitation of dimethylnitramine molecules was $\sim 12 \pm 3$ kcal/mol above the dissociation limit. Dimethylamino radical is the primary photofragment, undergoing mainly oxidation from parent dimethylnitramine molecules, leading to the two most important decomposition products, dimethylnitrosamine and formaldoxime. This oxidative reaction is very essential to the overall mechanism of dimethylnitramine decomposition and, furthermore, to the thermal degradation of nitramines. In general, amino radicals are primary decomposition products of nitramines and act as inhibitors of similar oxidation reactions that lead to their deterioration. Our results reveal also the presence of competing secondary reactions following the photodecomposition of dimethylnitramine. A complete understanding of their thermal or photochemical decomposition, especially in the case of more complex members of the series, will require knowledge of the detailed chemical kinetics and reaction dynamics of similar amino radical reactions. Finally, such studies provide valuable information about the nitramine decomposition chemistry and the thermal stability of energetic compounds.

*Acknowledgment.* This work was partly supported by the University of Crete Research Committee. Y.L. also acknowledges the support by the Zervas Foundation, Athens.

(21) Lindley, C. R. C.; Calvert, J. G.; Shaw, J. H. *Chem. Phys. Lett.* **1979**, *67*, 57.

# Shock Tube Study of the Reaction H + $O_2$ → OH + O Using OH Laser Absorption

**David A. Masten,* Ronald K. Hanson, and Craig T. Bowman**

*High Temperature Gasdynamics Laboratory, Department of Mechanical Engineering, Stanford University, Stanford, California 94305* *(Received: January 10, 1990; In Final Form: April 17, 1990)*

Mixtures of hydrogen and oxygen dilute in argon were heated by both incident and reflected shock waves to measure the rate coefficient of the $H_2/O_2$ mechanism branching reaction H + $O_2$ → OH + O (2) in the temperature range 1450–3370 K. Time histories of OH($X^2\Pi$) were monitored by using narrow-line-width laser absorption at 306.7 nm. A detailed kinetic analysis of the data in rich mixtures yielded the following rate coefficient expression: $k_2 = (9.33 \pm 0.40) \times 10^{13} \exp[-(14800 \pm 170)$ cal mol$^{-1}/RT$, K] cm$^3$ mol$^{-1}$ s$^{-1}$. In addition, H atom production was measured with atomic resonance absorption spectroscopy (ARAS) in incident shock experiments over the temperature range 1450–2152 K both simultaneously with OH detection and in separate experiments. The rate coefficient data obtained by ARAS are in excellent agreement with those based on the OH absorption but exhibit larger scatter. The rate coefficient derived from OH measurements lies 27–38% below the determination of Frank and Just (1985) at 1700–2500 K and agrees with that of Pirraglia et al. (1989), within their stated uncertainty, at overlapping temperatures of 1450–1705 K.

## Introduction

The chain-branching reaction H + $O_2$ → OH + O is one of the most important elementary gas-phase reactions in combustion. Under many conditions, it is the rate-controlling reaction in $H_2/O_2$ combustion, and it is also an integral part of all hydrocarbon oxidation mechanisms. Since the review of Baulch et al.,[1] it has been the subject of numerous high-temperature experimental investigations,[2-9] theoretical studies,[10-12] and subsequent reviews.[13-15] The near factor of 2 discrepancy in these recent experimental and theoretical studies is significant due to the sensitivity of ignition and flame propagation to this reaction.

With the advent of CW ring dye lasers as a narrow-line-width source of tunable radiation, quantitative and highly sensitive detection of several molecular radicals has become feasible in shock tube experiments.[16-20] This laser absorption approach was used here to monitor the OH concentration in the hydrogen–oxygen reaction.

The growth of the concentrations of the free radicals H, O, and OH in the $H_2/O_2$ reaction is primarily controlled by the chain-propagating and -branching reactions

(1) Baulch, D. L.; Drysdale, D. D.; Horne, D. G.; Lloyd, A. C. *Evaluated Data for High Temperature Reactions*; Butterworths: London, 1972; Vol. 1.
(2) Schott, G. L. *Combust. Flame* **1973**, *21*, 357.
(3) Chiang, C. C.; Skinner, G. B. *Twelfth Symposium (International) on Shock Tubes and Waves*; Magnes Press: Jerusalem, 1979; p 629.
(4) Pamidimukkala, K. M.; Skinner, G. B. *Thirteenth Symposium (International) on Shock Tubes and Waves*; SUNY Press: Albany, NY, 1980; p 585.
(5) Frank, P.; Just, Th. *Ber. Bunsen-Ges. Phys. Chem.* **1985**, *89*, 181.
(6) Fujii, N.; Shin, K. S. *Chem. Phys. Lett.* **1988**, *151*, 461.
(7) Vandooren, J.; da Cruz, F.; Nelson; Van Tiggelen, P. J. *Twenty-Second Symposium (International) on Combustion*; The Combustion Institute: Pittsburgh, 1988; p 1587.
(8) Pirraglia, A. N.; Michael, J. V.; Sutherland, J. W.; Klemm, R. B. *J. Phys. Chem.* **1989**, *93*, 282.
(9) Yuan, T.; Wang, C.; Rabinowitz, M. J.; Frenklach, M. Measurement of the Rate Coefficient of the Reaction H + $O_2$ → OH + O. Eastern States Section/Combustion Institute Meeting, Oct 1989.
(10) Miller, J. A. *J. Chem. Phys.* **1981**, *74*, 5120.
(11) Miller, J. A. *J. Chem. Phys.* **1986**, *84*, 6170.
(12) Troe, J. *J. Phys. Chem.* **1986**, *90*, 3485.
(13) Dixon-Lewis, G.; Williams, D. J. In *Comprehensive Chemical Kinetics*; Bamford, C. H., Tipper, C. F. H., Eds.; Elsevier: Amsterdam, 1977; Vol. 17.
(14) Warnatz, J. In *Combustion Chemistry*; Gardiner, Jr., W. C., Ed.; Springer-Verlag: New York, 1984; Chapter 5.
(15) Cohen, N.; Westberg, K. R. *J. Phys. Chem. Ref. Data* **1983**, *12*, 531.
(16) Hanson, R. K.; Salimian, S.; Kychakoff, G.; Booman, R. A. *Appl. Opt.* **1983**, *21*, 641.
(17) Louge, M. Y.; Hanson, R. K.; Rea, E. C.; Booman, R. A. *J. Quant. Spectrosc. Radiat. Transfer* **1984**, *32*, 353.
(18) Kohse-Höinghaus, K.; Davidson, D. F.; Chang, A. Y.; Hanson, R. K. *J. Quant. Spectrosc. Radiat. Transfer* **1989**, *42*, 1.
(19) Mertens, J. D.; Chang, A. Y.; Hanson, R. K.; Bowman, C. T. *Int. J. Chem. Kinet.* **1989**, *21*, 1049.
(20) Dean, A. J.; Hanson, R. K. *J. Quant. Spectrosc. Radiat. Transfer* **1989**, *42*, 375.

0022-3654/90/2094-7119$02.50/0 

$$OH + H_2 \rightarrow H_2O + H \quad (1)$$

$$H + O_2 \rightarrow OH + O \quad (2)$$

$$O + H_2 \rightarrow OH + H \quad (3)$$

after an initiation period where small concentrations of the radicals are produced. In the present work, the OH concentration time histories were monitored from the early near-exponential growth until the establishment of "plateau" concentrations which result from the partial equilibration of the above reactions. Detailed kinetic modeling was used to determine test gas mixtures such that the OH growth was sensitive to the rate coefficient of $H + O_2 \rightarrow OH + O$ almost exclusively. Both incident and reflected shock waves were utilized to determine $k_2$ over the extended temperature range 1450–3370 K.

In addition, hydrogen atom concentrations were monitored by using atomic resonance absorption spectroscopy (ARAS) in conjunction with the OH diagnostic in some of the incident shock experiments. The ARAS technique is more sensitive than laser absorption (owing to the larger values of absorption coefficients for atomic species), and thus H atom concentrations could be measured earlier in the reaction. Additional more dilute, incident shock wave experiments were conducted with H atom ARAS as the sole diagnostic to better utilize the higher sensitivity of this technique. H atom ARAS determinations of $k_2$ over the temperature range 1450–2152 K were in good agreement with $k_2$ based on OH absorption.

## Experimental Details

The experiments were conducted in a 15.24-cm-diameter stainless steel, pressure-driven shock tube with a 10.5-m-long driven section and 2.3-m-long driver section. The bakeable driven section was evacuated with a Varian V-1000 1000 L/s turbomolecular pump to an ultimate pressure of $5 \times 10^{-7}$ Torr and a leak-plus-outgassing rate of $2 \times 10^{-6}$ Torr min$^{-1}$ when pumped overnight. Experiments were performed with turnaround times of approximately 1 h with typical evacuated pressure of $2 \times 10^{-6}$ Torr and $10^{-5}$ Torr min$^{-1}$ leak-plus-outgassing rate. The driver section was evacuated with a mechanical pump through a zeolite sieve. Driver and driven sections were separated by aluminum diaphragms. Helium (Liquid Carbonic, 99.9% minimum purity) was used as the driver gas in all experiments.

Test gas mixtures were prepared by partial pressures in a bakeable 14-L stainless steel tank with magnetic stirrer. The mixing tank was evacuated by a mechanical pump and zeolite sieve combination with final pumping by the shock tube turbomolecular pump. Gases were fed into the driven section through the end wall of the tube. In most cases there was sufficient gas for multiple runs from one mixture. An MKS Baratron capacitance manometer was used to measure both the reactant pressures in the mixing tank (typically 2–50 Torr of $O_2$ and $H_2$ and 500–1000 Torr of Ar) and the initial test gas pressure $P_1$ in the shock tube (8–70 Torr) with a precision of better than 0.01 Torr for pressures under 100 Torr and 0.1 Torr for greater pressures.

Shock speeds were measured with a series of four platinum thin film gauges along the driven section. Shock passage actuated thin film pulses which were amplified and routed to a set of three time interval counters. Because of the desire for high accuracy in the determination of the rate coefficient of the title reaction, it is important to keep uncertainties in temperature, and therefore in shock velocity, to a minimum. The different response times of the thin films to the shock passage, as measured by the delay between the time of the initial resistance change of the film and the amplified pulse, were separately determined over the entire range of shock velocities. Corrections were then made for the different delays of the four films. With these corrections, the uncertainty in the shock velocities is estimated as ±0.2%, translating to temperature uncertainties of ±0.4%. Postshock pressures were monitored with a Kistler 603B1 pressure transducer and 5004 amplifier for the reflected shock experiments only. Typical shock attenuation was 1.0–1.5% m$^{-1}$.

The following gases were used in test mixtures throughout: $O_2$ (Air Products, ultrapure carrier grade, 99.994% purity), $H_2$ (Air Products, ultrapure carrier grade, 99.999% purity), Ar (Liquid Carbonics, research grade, 99.9995% purity), and $N_2O$ (Liquid Carbonics, 99.99% purity), all without further purification.

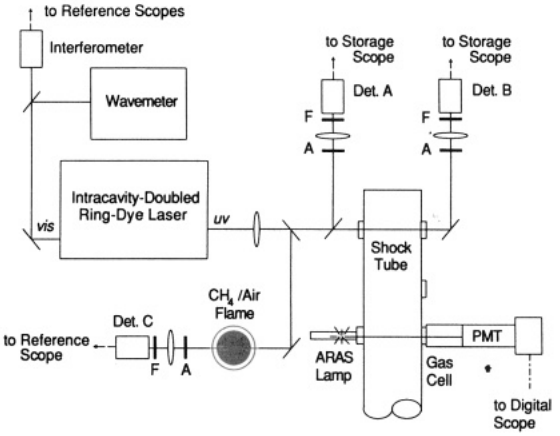


**Figure 1.** Experimental arrangement: solid lines, optical paths; dashed lines, electrical paths. A, aperture; F, filter (1-mm Schott UG-5).

*OH Experimental Arrangement.* OH was monitored by using the $R_1(5)$ line of the $A^2\Sigma^+ \leftarrow X^2\Pi_i$ system at 306.687 nm (vacuum). A Spectra-Physics 380 ring dye laser was intracavity frequency doubled using a temperature-tuned AD*A crystal (Spectra-Physics 398A). The laser was run with Rhodamine 590 dye and pumped with 3–4 W (all lines) from a Spectra-Physics 171 argon ion laser. Approximately 5 mW of single-mode UV power was obtained.

The laser was run without the galvo tuning rhomb assembly. In this mode, the laser wavelength can only be tuned to within one axial cavity mode (240 MHz) of the absorption line center. Line-shape calculations indicate that this is sufficient resolution (absorption coefficient within 1% of that at line center) for measurements at the experimental temperatures and pressures of the present study, where the OH $R_1(5)$ line width is a few gigahertz (fwhm). The wavelength of the visible output of the laser was monitored by a Burleigh WA-10 wavemeter. A methane/air flame also was used to ensure that the laser wavelength was at the OH absorption peak. The laser mode structure was monitored by passing a portion of the visible beam into a Spectra-Physics Model 470 scanning interferometer (8.00 GHz free spectral range (FSR)).

The experimental arrangement is shown in Figure 1. The UV beam is focused to an approximate diameter of 0.8 mm at the center of the shock tube through UV fused silica windows. The beam is sampled before and after entering the shock tube by using front-surface reflections from fused silica plates. The first beam splitter is set at an angle of 45° to sample approximately 10% of the beam. The angle of the second beam splitter is then adjusted so that the magnitudes of the signals from the two detectors are identical. This optical balancing eliminates the introduction of amplifier noise that would occur with electronic balancing. All detectors were amplified EG&G UV100BQ photodiodes (electronic 3-dB bandwidth of 150 kHz) masked with Schott UG-5 filters. The reference signal and difference (reference − probe) signal are then recorded on digital storage oscilloscopes (Nicolet 2090, with 0.5-μs sampling interval in most experiments). The noise on the optically balanced difference signal was typically 0.1–0.3% of the reference signal, approximately a 10-fold improvement over the noise on the reference signal alone.

In reflected shock wave experiments, the beam was located 2 cm from the end wall, while for the incident shock wave experiments, the beam was located 51 cm upstream of the end wall (10.0 m downstream from the diaphragm station). The ARAS detection system was located 30.5 cm upstream of this location.

*Hydrogen ARAS Experimental Arrangement.* The ARAS system is similar in design to that used by Chiang et al.[21] and

(21) Chiang, C. C.; Lifshitz, A.; Skinner, G. B.; Wood, D. R. *J. Chem. Phys.* **1979**, *70*, 5614.

Michael et al.[22] The light source consists of a 2.45-GHz microwave generator operating at 30 W coupled to a $^1/_4$ wave Evenson-Broida cavity which excites a microwave discharge in a 12-mm quartz tube containing a flowing mixture of 1% $H_2$ in He (Liquid Carbonics) at a pressure of 3 Torr. The radiation generated is primarily at the hydrogen resonance, Lyman-$\alpha$ wavelength (121.57 nm). This lamp is connected directly to the shock tube with a plane $MgF_2$ window fit as flush to the inner surface of the tube as practicable. $MgF_2$ transmits approximately 40% of the incident radiation at this wavelength. The radiation transmitted through the shock-heated gases was measured with an EMR solarblind UV photomultiplier Model 541G-09-18 with a sharply peaked 21% quantum efficienty at this wavelength. The photomultiplier was separated from the shock tube by a gas filter consisting of an 8-cm cell through which dry air flowed at atmospheric pressure. Oxygen absorbs most of the UV radiation emitted from the lamp while passing the Lyman-$\alpha$ radiation.[23] This cell was connected to the shock tube with an $MgF_2$ window. Slits 7 mm high and 3 mm wide (direction of shock propagation) were inserted next to the lamp and gas filter windows to collimate the beam and restrict shock transit time. With the use of the gas filter instead of a monochromator, a high signal-to-noise ratio of 50 was achieved with a time constant ($1/e$) of 3 $\mu$s.

*ARAS Calibration.* Calibration experiments were necessary to translate the records of Lyman-$\alpha$ absorption into corresponding H atom time histories. For temperatures above 2000 K, the calibrations were performed in mixtures of $H_2$ dilute in argon using the known dissociation rate of hydrogen.[1,14] At temperatures much below 2000 K, this reaction is too slow to generate sufficient H atoms. $N_2O/H_2/Ar$ mixtures were used for calibration in the temperature range 1500–2350 K, with H atoms produced primarily by the following sequence

$$N_2O + M \rightarrow N_2 + O + M$$
$$O + H_2 \rightarrow OH + H$$
$$OH + H_2 \rightarrow H_2O + H$$

with some contribution from the $H_2$ dissociation reaction above 2000 K. The complete calibration reaction mechanism is given in Table I. This is the same mechanism used for reducing data from the $H_2/O_2$ mixtures with reactions of N-containing species (reactions 20–23) added. In mixtures of a few ppm $N_2O$ and excess $H_2$, the H atom formation rate is controlled by the well-known rate of the initial $N_2O$ decomposition, with little sensitivity to subsequent reactions.

Background absorption by the initial reactants, as indicated by a reduction in Lyman-$\alpha$ signal immediately after shock passage, was observed in the calibration experiments. The data were corrected for this by reducing the reference intensity by the amount of background absorption observed after the shock passage. This absorption, primarily by $H_2$, is expected to be nearly constant due to the small time-dependent change in $H_2$ concentration. The $N_2O$ contribution to background absorption is small due to the low concentrations used in the calibration experiments. In the $H_2/O_2/Ar$ mixtures, where very large H atom concentrations are produced and thus complete absorption of the Lyman-$\alpha$ is expected at long reaction times, 98 ± 2% of the incident radiation was absorbed. This indicates the presence of only a small non-Lyman-$\alpha$ component of the radiation, a result consistent with separate monochromator scans of the output of the lamp, filter, photomultiplier tube combination. Neither calibration nor rate coefficient experimental data were adjusted for non-Lyman-$\alpha$ due to this small magnitude, where the effect of as much as a 4% non-Lyman-$\alpha$ component on the rate determination is less than 5% for all experiments. Calibrations were performed during the course of the investigation to ensure consistency of lamp operation between calibration and rate determination experiments. The adjusted absorption time histories were compared with H atom concentration histories calculated with the Chemkin[24] kinetics code to generate calibration curves of H atom concentration vs absorbance.

The H atom calibration approximated Beer's law behavior for small fractional absorption with a deviation toward lower sensitivity at greater absorption. The initial absorption cross section, $\sigma$, defined as

$$\sigma = \ln (I_0/I)/[H]l \quad \text{cm}^2\ \text{mol}^{-1}$$

was calculated for each calibration experiment and is shown in Figure 2a. Agreement between the two calibration methods is well within the approximate ±30% scatter in the overlapping temperature range. The uncertainty in the cross-section determination from the $H_2/Ar$ calibration experiments can be no better than the uncertainty in the rate coefficient of the dissociation of $H_2$. This rate coefficient is considered to be known within a factor of 2,[14] and therefore the calibration results derived agree with the $N_2O/H_2/Ar$ calibrations well within the rate coefficient uncertainties.

The cross section calculated from the calibration measurements changes only approximately 30% over the temperature range of the present experiments. Since this falls within the scatter of the cross-section data and the uncertainty in the $N_2O$ and $H_2$ dissociation rates, an averaged calibration curve representative of a temperature near the mean of the $H_2/O_2$ experiments, including the non Beer's law behavior at higher absorption, was used to reduce all the H atom ARAS data (see Figure 2b).

**TABLE I: Reaction Mechanism; Rate Coefficients in the Form $k_j = AT^B \exp(-E_a/RT)$[a]**

| reaction | $A$ | $B$ | $E_a$ | ref |
|---|---|---|---|---|
| 1. OH + $H_2$ = $H_2O$ + H | $1.17 \times 10^9$ | 1.3 | 3626 | 13 |
| 2. H + $O_2$ = OH + O | $9.33 \times 10^{13}$ | 0.0 | 14800 | *b* |
| 3. O + $H_2$ = OH + H | $5.06 \times 10^4$ | 2.67 | 6290 | 48 |
| 4. OH + OH = O + $H_2O$ | $6.00 \times 10^8$ | 1.3 | 0 | 49 |
| 5. O + $HO_2$ = $O_2$ + OH | $1.40 \times 10^{13}$ | 0.0 | 1073 | 49 |
| 6. H + $HO_2$ = OH + OH | $1.40 \times 10^{14}$ | 0.0 | 1073 | 49 |
| 7. H + $HO_2$ = $H_2$ + $O_2$ | $1.25 \times 10^{13}$ | 0.0 | 0 | 49 |
| 8. OH + $HO_2$ = $H_2O$ + $O_2$ | $7.50 \times 10^{12}$ | 0.0 | 0 | 49 |
| 9. $HO_2$ + $HO_2$ = $H_2O_2$ + $O_2$ | $2.00 \times 10^{12}$ | 0.0 | 0 | 50 |
| 10. $H_2O_2$ + OH = $H_2O$ + $HO_2$ | $1.00 \times 10^{13}$ | 0.0 | 1800 | 1 |
| 11. $H_2O_2$ + H = $H_2O$ + OH | $1.00 \times 10^{13}$ | 0.0 | 3600 | 14 |
| 12. $H_2O_2$ + H = $HO_2$ + $H_2$ | $1.60 \times 10^{12}$ | 0.0 | 3800 | 49 |
| 13. $H_2O_2$ + O = $HO_2$ + OH | $2.80 \times 10^{13}$ | 0.0 | 6400 | 14 |
| 14. $H_2O_2$ + M = OH + OH + M | $1.30 \times 10^{17}$ | 0.0 | 45500 | 14 |
| 15. O + O + M = $O_2$ + M | $1.89 \times 10^{13}$ | 0.0 | −1788 | 49 |
| 16. H + OH + M = $H_2O$ + M<br>$H_2O/5.0$[c] | $1.60 \times 10^{22}$ | −2.0 | 0 | 49 |
| 17. $H_2$ + M = H + H + M<br>$H_2/4.0/H_2O/18.6$[c] | $2.20 \times 10^{14}$ | 0.0 | 96000 | 14 |
| 18. H + $O_2$ + M = $HO_2$ + M<br>$H_2O/18.6/H_2/2.9$[c] | $3.61 \times 10^{17}$ | −0.72 | 0 | 49 |
| 19. H + O + M = OH + M<br>$H_2O/5.0$[c] | $6.20 \times 10^{16}$ | −0.6 | 0 | 49 |
| 20. $N_2O$ + M = $N_2$ + O + M[d] | $9.30 \times 10^{14}$ | 0.0 | 59465 | 5 |
| 21. $N_2O$ + O = NO + NO[d] | $6.92 \times 10^{13}$ | 0.0 | 26600 | 51 |
| 22. $N_2O$ + O = $N_2$ + $O_2$[d] | $1.00 \times 10^{14}$ | 0.0 | 28000 | 51 |
| 23. $N_2O$ + H = $N_2$ + OH[d] | $7.60 \times 10^{13}$ | 0.0 | 15100 | 51 |

[a] Units are mol, cm, s, K, and cal/mol. [b] This work. [c] Enhanced third-body efficiencies. [d] Used in H atom ARAS calibration only.

## Results

*OH Absorption Measurements.* A typical OH concentration profile for a shock-wave-heated $H_2/O_2$ mixture, shown in Figure 3, illustrates features common to most of the experimentally determined OH time histories. After an initiation period where small concentrations of the chain carriers H, O, and OH are formed, the growth of the OH concentration (as well as H atom and O atom concentrations) proceeds rapidly and is controlled

(22) Michael, J. V.; Sutherland, J. W.; Klemm, R. B. *Int. J. Chem. Kinet.* **1986**, *17*, 315.
(23) Appel, D.; Appleton, J. P. *Fifteenth Symposium (International) on Combustion*; The Combustion Institute: Pittsburgh, 1975; p 701.
(24) Kee, R. J.; Miller, J. A.; Jefferson, T. H. Chemkin: A General-Purpose Problem-Independent, Transportable, Fortran Chemical Kinetics Code Package. Report No. SAND80-8003; Sandia National Laboratory: Albuquerque, NM, 1980.

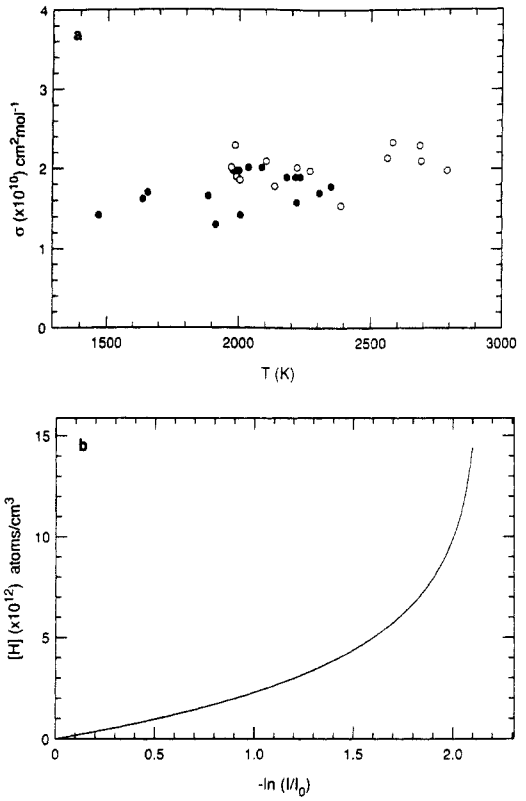


**Figure 2.** (a) H atom ARAS calibration. Plot of Beer's law regime absorption cross section vs temperature: solid circles, $N_2O/H_2/Ar$ mixtures; open circles, $H_2/Ar$ mixtures. (b) H atom ARAS calibration curve used for all ARAS data reduction. H atom concentration vs absorbance.

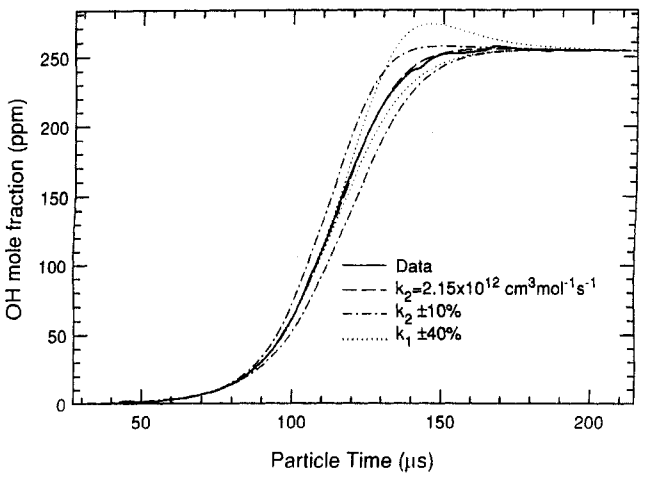


**Figure 3.** Comparison of experimental and Chemkin calculated OH profiles using best-fit $k_2$ with effect of ±10% variation on $k_2$ (incident shock, $T$ = 1980 K, $P$ = 0.675 atm, 5.0% $H_2$, 0.493% $O_2$). Dotted curves indicate effect of ±40% variation of $k_1$ used in Table I.

primarily by the chain-propagating and -branching reactions 1–3. This period of rapid radical growth is terminated by the partial equilibration of reactions 1–3, resulting (for most experimental conditions) in plateau levels of the chain carrier concentrations. The rate coefficient $k_2$ was determined by fitting the region of rapid OH evolution.

The OH concentration profiles were calculated from the recorded absorption and reference signals by using Beer's law, with absorption coefficients calculated by using the method described in Goldman and Gillis[25] and the known line position,[25] Einstein coefficient,[25] and pressure broadening coefficients.[26] This method has been used previously and was shown to agree with calculated plateau levels to ±5%.[16] Typical detection limits (S/N = 1) ranged from 0.5 to 5 ppm, with plateau concentrations from 60 to over 1000 ppm.

**TABLE II: Experimental Conditions and Results for OH Absorption**

| $T$, K | $P$, atm | $\rho$ (×10$^{-5}$), mol cm$^{-3}$ | $H_2$, mol % | $O_2$, mol % | $k_2$ (×10$^{12}$), cm$^3$ mol$^{-1}$ s$^{-1}$ |
|---|---|---|---|---|---|
| | | Incident Shock Waves | | | |
| 1449 | 1.457 | 1.225 | 2.54 | 0.492 | 0.601 |
| 1452 | 1.461 | 1.226 | 4.99 | 0.500 | 0.577 |
| 1518 | 0.886 | 0.711 | 5.04 | 0.500 | 0.683 |
| 1579 | 1.000 | 0.772 | 4.96 | 0.492 | 0.826 |
| 1589 | 0.606 | 0.465 | 4.97 | 0.496 | 0.850 |
| 1635 | 1.100 | 0.820 | 3.18 | 0.317 | 0.971 |
| 1710 | 0.461 | 0.329 | 2.14 | 0.212 | 1.25 |
| 1806 | 0.638 | 0.431 | 4.08 | 0.400 | 1.50 |
| 1813 | 0.666 | 0.448 | 2.55 | 0.477 | 1.56 |
| 1823 | 0.708 | 0.473 | 4.08 | 0.400 | 1.47 |
| 1980 | 0.675 | 0.416 | 5.00 | 0.493 | 2.15 |
| 1986 | 0.599 | 0.368 | 2.14 | 0.212 | 2.31 |
| 2028 | 0.479 | 0.288 | 4.97 | 0.496 | 2.49 |
| 2172 | 0.565 | 0.317 | 4.96 | 0.492 | 3.00 |
| 2206 | 0.432 | 0.239 | 4.97 | 0.496 | 3.34 |
| 2408 | 0.672 | 0.340 | 3.18 | 0.317 | 4.21 |
| 2701 | 0.358 | 0.162 | 4.97 | 0.496 | 6.22 |
| 2734 | 0.379 | 0.169 | 3.18 | 0.317 | 6.42 |
| | | Reflected Shock Waves | | | |
| 1960 | 2.525 | 1.570 | 1.82 | 0.181 | 1.84 |
| 2041 | 2.383 | 1.423 | 1.10 | 0.208 | 2.36 |
| 2105 | 2.644 | 1.531 | 1.945 | 0.199 | 2.47 |
| 2151 | 2.442 | 1.384 | 0.964 | 0.200 | 2.78 |
| 2234 | 2.189 | 1.194 | 0.906 | 0.168 | 3.23 |
| 2298 | 2.279 | 1.209 | 0.906 | 0.168 | 3.53 |
| 2386 | 2.345 | 1.198 | 1.82 | 0.181 | 3.86 |
| 2616 | 2.037 | 0.949 | 0.461 | 0.046 | 5.39 |
| 2681 | 2.083 | 0.947 | 1.014 | 0.215 | 5.77 |
| 2769 | 1.991 | 0.876 | 0.964 | 0.200 | 6.31 |
| 2898 | 1.984 | 0.834 | 1.10 | 0.208 | 7.11 |
| 3370 | 1.590 | 0.575 | 0.709 | 0.122 | 10.80 |

The test conditions and results of incident shock wave experiments in $H_2/O_2/Ar$ mixtures using the OH diagnostic are given in Table II. Incident shock temperatures and pressures ranged from 1449 to 2734 K and 0.33 to 1.46 atm, respectively. Mixtures with nominally stoichiometric ratios of $H_2/O_2$ = 2:1 and rich ratios, nominally 5:1 and 10:1, were used. These mixtures were selected with the aid of computer simulations using the reaction mechanism of Table I and the Chemkin[24] and Senkin[27] kinetics codes, with the aim of maximizing the sensitivity of the OH growth to the rate coefficient of reaction 2. Figure 4 shows representative OH sensitivity analyses for a rich mixture and for a stoichiometric mixture. The sensitivity coefficient $\alpha$, calculated in Senkin,[27] is the partial derivative of a species mole fraction with respect to the rate constant parameter $A$ of a reaction, normalized by the maximum species mole fraction and the rate constant parameter $A$

$$\alpha_{ij}(t) = (A_i/X_j^{max})(dX_j/dA_i)$$

where $X_j$ is the mole fraction of species $j$ and $A_i$ is the temperature-independent factor of the rate constant of reaction $i$. The analysis indicates that the OH profile is most sensitive to the rate coefficient of the reaction $H + O_2 \rightarrow OH + O$. However, there is some sensitivity to the rate coefficients of reactions 1 and 3, and reaction 7, the initiation reaction for most experimental conditions. Computer modeling indicated that variation of the rate coefficient $k_7$ influences the length of the induction period only, where the induction time is defined as the time between shock passage and first measurable OH concentration. Variation of $k_7$

(25) Goldman, A.; Gillis, J. R. *J. Quant. Spectrosc. Radiat. Transfer* **1981**, *25*, 111.

(26) Rea, E. C., Jr.; Chang, A. Y.; Hanson, R. K. *J. Quant. Spectrosc. Radiat. Transfer* **1987**, *37*, 117.

(27) Lutz, A. E.; Kee, R. J.; Miller, J. A. Senkin: A Frotran Program for Predicting Homogeneous Gas Phase Chemical Kinetics with Sensitivity Analysis. Report No. SAND87-8248; Sandia National Laboratory: Albuquerque, NM, 1988.

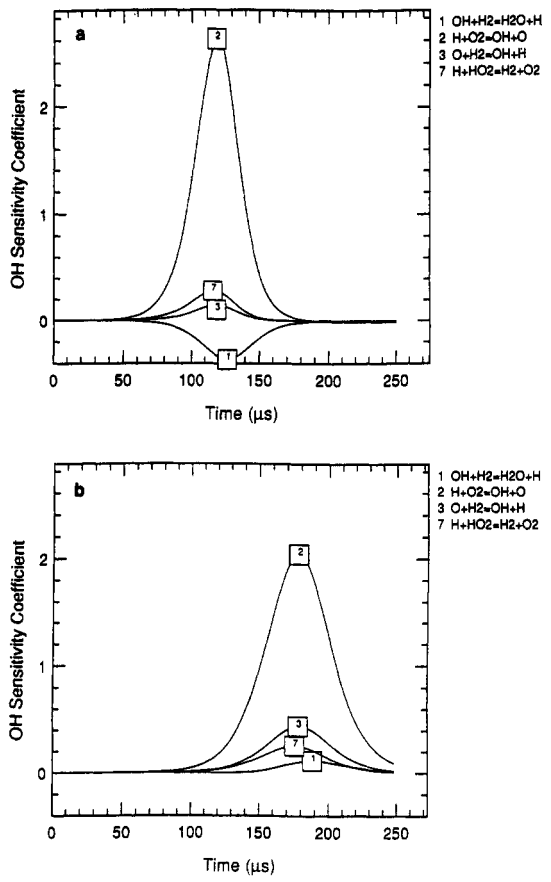


**Figure 4.** (a) Sensitivity plot for OH conditions of Figure 3 (rich mixture). (b) Sensitivity plot for OH for an example stoichiometric mixture ($T$ = 1980 K, $P$ = 0.675 atm, 1.0% $H_2$, 0.493% $O_2$).

by a factor of 3 produced no change in the calculated rate of growth of the OH concentration for any of the experimental conditions used in the present study; therefore, the uncertainty in the rate coefficient of reaction 7 does not introduce any uncertainty in the determination of $k_2$. The addition of an alternative initiation reaction, $H_2 + O_2 \rightarrow 2OH$, also influenced the computed induction time only, with no effect on the postinduction rate of growth of the OH concentration.

Comparison of sensitivity analyses over the full range of test temperatures indicated that the sensitivity to $k_3$ is greater for stoichiometric mixtures, while the sensitivity to $k_1$ is greater for rich mixtures. Since the effect of the combined estimated uncertainties of the rate coefficients of reactions 1 and 3 on the $k_2$ determination is approximately a factor of 2 greater for the stoichiometric experiments compared to the rich mixture experiments, the majority of the experiments were conducted with rich mixtures and were used exclusively in the rate determination. The rate chosen for reaction 1[13] lies within ±15% of the recent three-parameter expressions of Oldenborg et al.[28] and Michael and Sutherland[29] and within 30% of the two-parameter expressions of Davidson et al.[30] and Frank and Just[5] for the present temperature range. The contribution to the uncertainty in $k_2$ from an uncertainty in $k_1$ of as much as the recommended ±40%[14] is less than ±5% for the experimental conditions utilized.

The data were modeled with the reaction mechanism in Table I (without the nitrogen species reactions 20–23) using the Chemkin[24] and Senkin[27] computer codes and the Sandia National Laboratories thermodynamic data base.[31] The codes require the input of assumptions of the thermodynamic state of the postshock mixture in order to account for state changes due to reaction exothermicity. Constant internal energy and specific volume were assumed for both incident and reflected shock wave experiments, and this was checked against the assumption of constant enthalpy and pressure for a number of experimental conditions. Agreement in calculated OH mole fraction was within ±1% with both assumptions. The mixtures utilized were sufficiently dilute such that Chemkin[24] calculated postshock temperatures typically increased less than 1% between shock passage and establishment of partial equilibrium (plateau OH concentration) due to reaction exothermicity. Time-dependent corrections in the absorption coefficient arising from this temperature change were included (also near 1%). Absorption coefficient sensitivity to evolving species concentrations, such as the line broadening contributions due to $H_2O$ formation, was found to be negligible.

As a first step in the data analysis, for the experiments where a definite OH plateau was observed, the experimentally determined OH plateau concentrations were compared to the Chemkin calculated partial equilibrium levels. Agreement was very good, within ±2% for most cases and within ±5% for all. This calculated partial equilibrium OH concentration is a function of the reactant concentrations, pressure, temperature, thermochemical data, and recombination reaction rate coefficients. Therefore, the minor differences between measured and Chemkin calculated plateaus could be due to a combination of uncertainties in these quantities and the absorption coefficient uncertainties. The calculated plateau OH concentrations showed little or no dependence on the rate coefficients of any reactions in Table I when varied within reasonable uncertainties. For the data reduction, we chose to treat the experiments as self-calibrating and matched the experimentally determined and Chemkin calculated plateaus, in effect making small corrections to the calculated absorption coefficients (within the above-mentioned ±5%).

The rate coefficient of reaction 2 was then determined by varying $k_2$ in the mechanism of Table I until the difference between measured and Chemkin calculated OH concentration was minimized in the regime bounded by the first detectable OH concentration and the OH plateau. The induction time was then matched by varying the rate coefficient of the initiation reaction $k_7$. Iteration with the best-fit $k_7$ confirmed no change in the best-fit $k_2$. This procedure allowed a $k_2$ determination independent of the initiation reaction uncertainties because of the previously mentioned insensitivity of the postinduction OH profile to the identity or rate coefficient of the initiation reaction.

Figure 3 shows a calculated best fit of the experimental OH profile and the effect of varying $k_2$ by ±10%. Figure 4a, the sensitivity analysis for the conditions of Figure 3, indicates that the OH profile is most sensitive to reaction 2 and that reaction 1 is the next most important. Also shown in Figure 3 is the effect of varying the rate of reaction 1 by its estimated uncertainty, ±40%. The effect of the uncertainty in $k_1$ on the final $k_2$ determination is small (±4% on $k_2$ for a ±40% variation in $k_1$). The effect of varying all other rates within their uncertainties for this set of conditions is negligible.

The test conditions and results of the reflected shock wave experiments are given in Table II. Reflected shock temperatures and pressures ranged from 1960 to 3370 K and 1.59 to 2.64 atm, respectively. Only rich mixtures with nominal $H_2/O_2$ ratios of 5:1 and 10:1 were used. Sensitivity analysis indicated that for these experiments the isolation of reaction 2 as the dominant reaction required somewhat less rich mixtures than in the lower pressure and temperature incident shock wave mixtures. This is due to the increasing contribution of $H_2$ dissociation, reaction 17, to the radical production in rich mixtures at high temperature. The increasing contribution of dissociation reactions to the OH growth rate eventually limits the high-temperature end of this study.

(28) Oldenborg, R. C.; Harradine, D. M.; Loge, G. W.; Winn, K. R. Kinetic Study of the OH + $H_2$ Reaction from 800 to 1550 K. Presented at the Second International Conference on Chemical Kinetics, National Institute of Standards and Technology, Gathersburg, MD, July 24–27, 1989.

(29) Michael, J. V.; Sutherland, J. W. *J. Phys. Chem.* **1988**, *92*, 3853.

(30) Davidson, D. F.; Chang, A. Y.; Hanson, R. K. *Twenty-Second Symposium (International) on Combustion*; The Combustion Institute: Pittsburgh, 1988; p 1877.

(31) Kee, R. J.; Rupley, F. M.; Miller, J. A. The Chemkin Thermodynamic Data Base. Report No. SAND87-8215; Sandia National Laboratory: Albuquerque, NM, 1987.

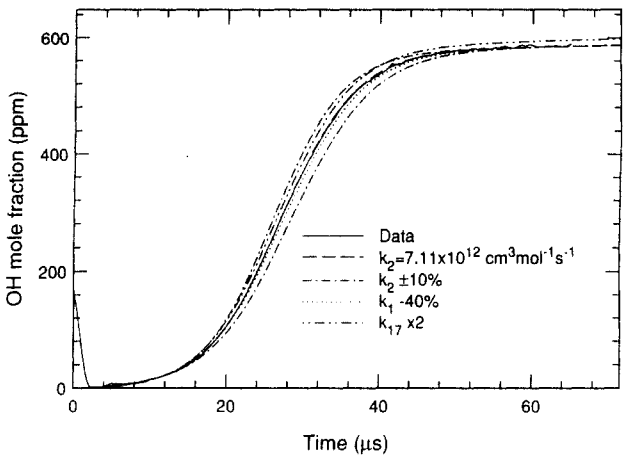


**Figure 5.** Comparison of experimental and Chemkin calculated OH profiles using best-fit $k_2$ with effects of variation of selected rate coefficients (reflected shock, $T$ = 2898 K, $P$ = 1.98 atm, 1.10% $H_2$, 0.208% $O_2$).

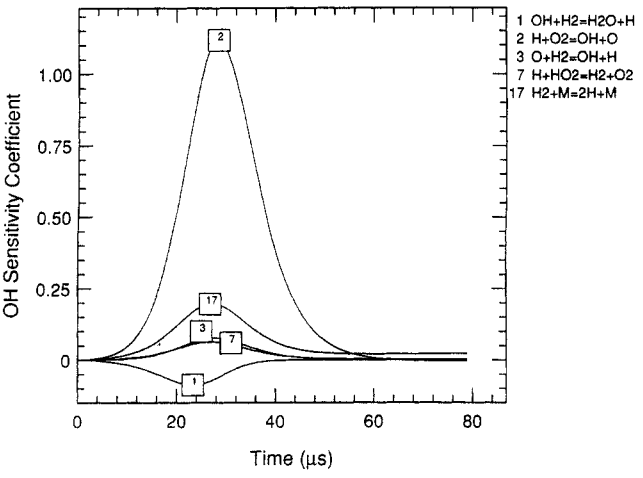


**Figure 6.** Sensitivity plot for OH for conditions of Figure 5.

A typical reflected shock wave OH absorption profile near the high-temperature extreme of our data is shown in Figure 5, with a corresponding sensitivity analysis given in Figure 6. The effects of variation of the rates of the most important interfering reactions, (1) and (17), are shown to be small. The experimentally determined and Chemkin calculated plateau OH concentrations agreed within 1%.

An Arrhenius plot of the OH laser absorption derived data from the rich mixtures only is given in Figure 7. The solid line is a least-squares fit to the combined incident and reflected shock rich mixture data

$$k_2 = (9.33 \pm 0.40) \times 10^{13} \exp[-(14800 \pm 170) \text{ cal mol}^{-1}/RT, \text{ K}] \quad \text{cm}^3 \text{ mol}^{-1} \text{ s}^{-1}$$

with incident and reflected data agreement within 5%. The standard deviation of the experimentally measured rate constants from the best-fit expression is ±5%. The stoichiometric mixture data yielded a rate coefficient approximately 10% greater than the above expression. Since the OH profiles from the stoichiometric mixtures are more sensitive to secondary reactions, particularly

$$O + H_2 \rightarrow OH + H \qquad (3)$$

the rich mixture data only were used for the rate determination as the contribution of all secondary reactions to the uncertainty is less than ±5%.

*Hydrogen ARAS Measurements.* Hydrogen atom production was monitored in the above incident shock wave experiments with the ARAS system. As these mixtures were designed for the OH diagnostic and contained relatively high reactant concentration,

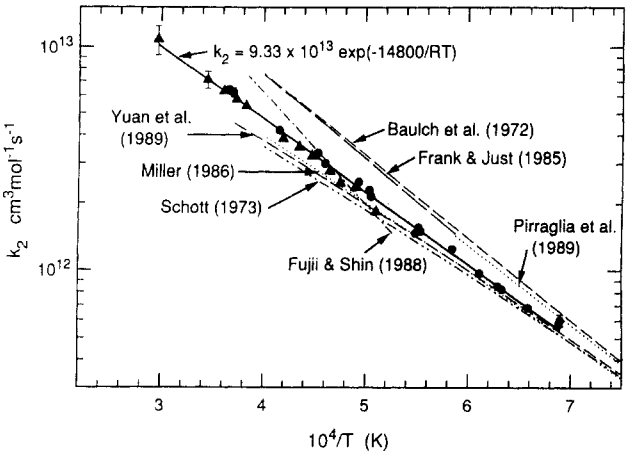


**Figure 7.** Arrhenius plot of rate coefficients for reaction 2, H + $O_2$ → OH + O, determined from OH absorption experiments: solid line, rate coefficient derived from OH data; circles, incident shock data; triangles, reflected shock data. Also shown are results from other recent determinations of $k_2$.

**TABLE III: Experimental Conditions and Results for H Atom ARAS Incident Shock Waves**

| $T_2$, K | $P_2$, atm | $\rho_2$ (×10$^{-5}$), mol cm$^{-3}$ | $H_2$, mol % | $O_2$, mol % | $k_2$ (×10$^{12}$), cm$^3$ mol$^{-1}$ s$^{-1}$ |
|---|---|---|---|---|---|
| 1452 | 1.46 | 1.226 | 4.99 | 0.500 | 0.44 |
| 1575 | 0.849 | 0.657 | 0.99 | 0.102 | 1.05 |
| 1579 | 1.00 | 0.772 | 4.96 | 0.492 | 0.65 |
| 1635 | 1.10 | 0.820 | 3.18 | 0.317 | 0.83 |
| 1700 | 0.794 | 0.569 | 0.99 | 0.103 | 1.15 |
| 1710 | 0.461 | 0.329 | 2.14 | 0.212 | 1.40 |
| 1740 | 0.809 | 0.567 | 1.12 | 0.498 | 0.73 |
| 1765 | 0.694 | 0.479 | 0.53 | 0.055 | 1.55 |
| 1784 | 0.890 | 0.615 | 1.98 | 0.197 | 1.65 |
| 1813 | 0.666 | 0.448 | 2.55 | 0.477 | 1.50 |
| 1823 | 0.717 | 0.479 | 0.99 | 0.103 | 1.70 |
| 1835 | 0.459 | 0.305 | 1.41 | 0.619 | 1.27 |
| 2011 | 0.630 | 0.382 | 0.99 | 0.103 | 2.40 |
| 2152 | 0.525 | 0.297 | 0.53 | 0.055 | 2.75 |

in most cases there was fast absorption of the ARAS signal on the order of the electronic response time of 3 μs. Only those runs where the time to reach 60% absorption exceeded 10 μs were reduced. Additional incident shock experiments with more dilute mixtures and thus lower H atom concentrations were run with ARAS only. All test conditions of the ARAS experiments and results are presented in Table III.

The rate coefficient $k_2$ was determined by using the methodology of Chiang and Skinner.[3] The ARAS measurements were used at early reaction times, well before the H atom concentration reaches partial equilibrium values. In this region, where reactant concentrations and shock conditions are essentially unperturbed from the initial postshock values, the radical concentrations are expected to increase exponentially after an initial induction period with a rate

$$[R] = [R]_0 \exp(\lambda t)$$

where [R] is the concentration of O, H, or OH. It has been shown that the growth constant λ is primarily a function of $k_2$ for rich mixtures, approaching

$$\lambda = 2k_2[O_2]$$

for infinite $H_2$:$O_2$ ratio and negligible recombination reaction rates.[32] For most of the conditions employed here, H atom ARAS data showed the expected exponential behavior. A sample trace is given in Figure 8 with both linear and logarithmic plots of H atom mole fraction vs time. The rate coefficient $k_2$ was varied to best fit the growth rate given as the inverse slope of the log-

(32) Brokaw, R. S. *Tenth Symposium (International) on Combustion*; The Combustion Institute: Pittsburgh, 1965; p 269.

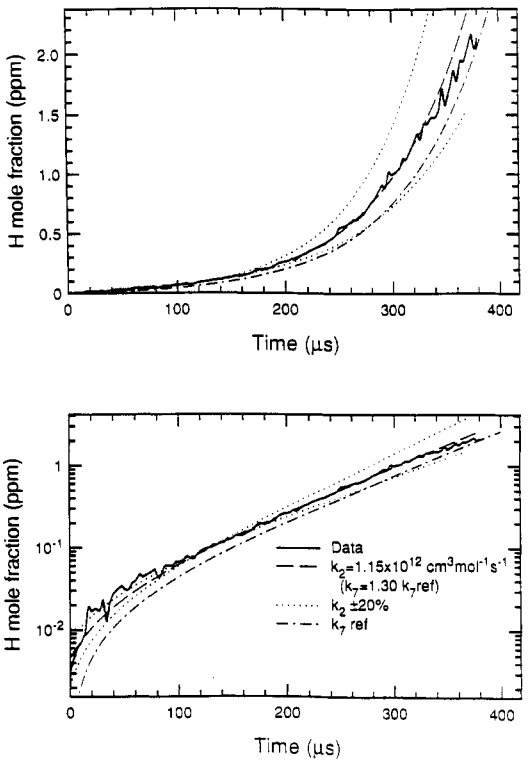


**Figure 8.** Comparison of experimental and Chemkin calculated H atom profiles using best-fit $k_2$ (incident shock, $T$ = 1700 K, $P$ = 0.794 atm, 0.99% $H_2$, 0.103% $O_2$). Dotted curves indicate effect of ±20% variation in $k_2$. Lower plot: the linear slope of the log of the H atom mole fraction indicates the early exponential growth of the H atom concentration. Variation of the rate coefficient of the initiation reaction (reaction 7) by 30% provides a match of the induction time but does not affect the slope or the $k_2$ determination.

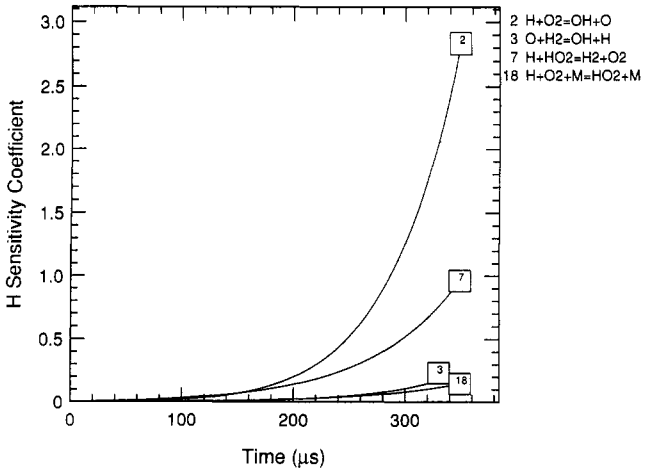


**Figure 9.** Sensitivity plot for H atom for the conditions of Figure 8.

arithmic plot. It was necessary to vary the initiation rate $k_7$ to match the absolute H atom concentrations. However, varying $k_7$ does not affect the slope of the logarithmic H atom profile and thus does not affect the $k_2$ rate coefficient determination. Figure 9 is a sensitivity plot showing the relative insensitivity of the H atom profile to other reactions. In a recent analysis of the $H_2$–$O_2$ reaction, Yetter et al.[33] cautioned that care must be exercised in this type of analysis at high temperature as the radical growth is not strictly exponential. The modeling of our highest temperature ARAS experiment ($T$ = 2152 K) did indicate a slowly decreasing growth constant, changing less than 15% over our short reaction time.

(33) Yetter, R. A.; Vajda, S.; Dryer, F. L. On the High Temperature Rate Constant Measurements of H + $O_2$ → OH + O. *Int. J. Chem. Kinet.*, to be published.

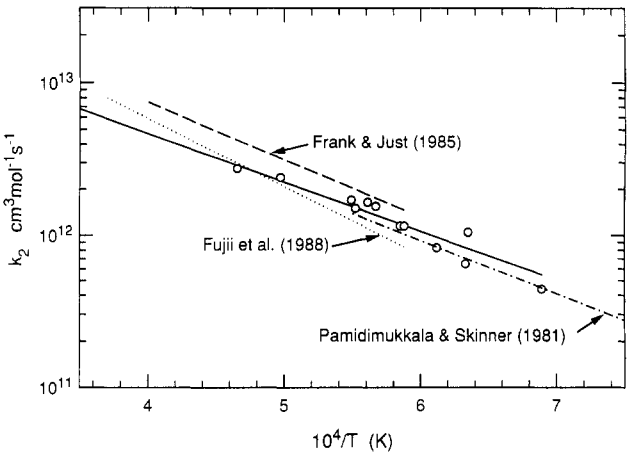


**Figure 10.** Arrhenius plot of rate coefficients for reaction 2, H + $O_2$ → OH + O, determined from H atom ARAS experiments. Solid line: rate coefficient expression derived from OH data. Also shown are three recent $k_2$ determinations using ARAS measurements.

The rate coefficient determinations from the H atom ARAS data are plotted in Figure 10 and are compared to the above rate coefficient expression. The agreement with the OH absorption $k_2$ determination is good, well within the approximately 40% scatter of the ARAS measurements.

*Uncertainty Analysis.* The effects of boundary layer development, vibrational nonequilibrium, and finite detection system response time on the OH absorption experiments were investigated and found to have negligible impact on the results.

The importance of considering the role of boundary layer growth on the determination of rate coefficients in incident shock wave experiments has been strongly emphasized.[34] With this in mind, one approach to limit the influence of boundary layer growth in incident shock wave experiments is to minimize the test time. In nearly all of the runs, the OH reached plateau concentrations within 100 μs after shock passage. The boundary layer development in the present experiments was characterized following the procedure of de Boer and Miller.[35] Laminar boundary layers were assumed, as should be the case in the lower temperature shocks used in the present experiments. This assumption provides an upper limit estimate of the boundary layer effect. The combined temperature perturbation due to the boundary layer "sink effect" and to shock attenuation (1.0–1.5% m$^{-1}$) was calculated to be approximately 1% of $T_2$ for the worst case. Flower[36] compared the long-term temperature behavior of the shock tube used in the present study to the theory of Mirels,[37-39] by examining the change in CO IR emission over long test times. He concluded that the theory greatly overpredicted the temperature changes. Recent CO emission tests near 2300 K confirm this, exhibiting less than a 0.3% temperature increase in 300 μs. Hence, it is concluded that boundary layer temperature effects in our shock tube, at the short test times employed, are negligible.

The effect of finite detector electronic rise time (1 μs) and shock transit time (1 μs) on the OH absorption determination of $k_2$ was investigated and found to be minimal. This potential effect was of concern, as the early near-exponential growth rate of the OH concentration, $1/\lambda$ (as defined for ARAS measurements), was typically 6–10-μs lab time in the incident shock wave experiments. However, the observation time, as measured by the interval from the first detectable OH to peak OH concentration, is somewhat

(34) Belles, F. E.; Brabbs, T. A. *Thirteenth Symposium (International) on Combustion*; The Combustion Institute: Pittsburgh, 1971; p 165.

(35) de Boer, P. C. T.; Miller, J. A. *Tenth Symposium (International) on Shock Tubes and Waves*; The Shock Tube Research Society: Kyoto, Japan, 1975; p 796.

(36) Flower, W. L. Ph.D. Thesis, Department of Mechanical Engineering, Stanford University, HTGL Report No. 103, 1976. Thesis, Department of Mechanical Engineering, Stanford University, HTGL Report No. 103, 1976.

(37) Mirels, H. *Phys. Fluids* **1963**, *6*, 1201.

(38) Mirels, H. *AIAA J.* **1964**, *2*, 84.

(39) Mirels, H. *Phys. Fluids* **1966**, *9*, 1907.

longer, varying from approximately 20- to 40-$\mu$s lab time. The effect was investigated by numerically convolving a smoothed model of experimental OH laser signals incident on the detection system with the known time response of the detection system. The resultant transformed signal was compared to the original modeled signal by reducing both to OH concentration time histories. It was found that the induction time was lengthened by 1 $\mu$s and the OH growth rate was reduced less than 2% for the worst case (at high temperatures and large reactant concentrations), which is within the uncertainty of the individual measurements.

The reflected shock wave experiments were designed to have slower OH growth rates (in the laboratory time frame) than the incident shocks and are not expected to be subject to strong boundary layer perturbations due to the close proximity of the end wall. Agreement between incident and reflected rate determinations confirms the small role of detector response time, shock transit time, and boundary layers.

An estimate was made of the possible contribution of vibrational nonequilibrium to the uncertainty in the determination of the rate coefficient of reaction 2. The reaction mechanism, Table I, was altered to include rate coefficients for reactions 1–3 and 7 with $H_2$, $O_2$, and OH in both the ground and first excited vibrational states. Relaxation rates for $H_2$[40] and $O_2$[41] were taken from the literature and were modified to Arrhenius form for inclusion in the reaction mechanism. The OH relaxation rate was taken from a theoretical calculation[42] and resulted in fast (<1 $\mu$s) OH vibrational relaxation. Conservatively high ratios of the excited-state to ground-state rate coefficients were used to investigate the possible effects of nonequilibrium. The excited-state rate coefficients of reactions 1 and 3 were assumed to be enhanced by a factor of 10 over the ground-state rate coefficients. This enhancement of reaction 1 is similar to the recommendation of Zellner[43] for the temperature range considered here. The factor of 10 enhancement by the excited-state $H_2$ for reaction 3 is approximately a factor of 2 larger than that used by Brown[44] in a similar investigation of vibrational effects. The enhancement of reaction 2 was assumed to follow the empirical formulation of Birely and Lyman:[45]

$$k_v/k_0 = \exp(aE_v/RT)$$

Here, $E_v$ is the vibrational energy of the excited species (in this case $H_2$) and $a$ is the fractional contribution of the vibrational energy that is effectively utilized to reduce the reaction barrier. The maximum value of unity was used for $a$. The resulting OH growth rates were 1–2% slower than for the case of instantaneous relaxation (equilibrium) of all three species, suggesting that a 1–2% upward compensation in $k_2$ would be needed to account for vibrational relaxation rates. These effects were due to the finite $O_2$ relaxation rate. Owing to its small magnitude and the many assumptions embedded in the analysis, such a correction was not included in the recommended result for $k_2$.

The possible effects of impurities were investigated by adding small initial concentrations (a few ppm) of H, O, OH, or $H_2O$ to computer-simulated experiments. The impurities influenced the computed induction time only, with no effect on the postinduction rate of growth of the OH concentration. The data reduction methodology used here is independent of the induction time and is thus not influenced by the expected small impurity level. Furthermore, shock-heated pure Ar showed no ARAS absorption noticeable above the typical 2% noise of the signal, indicating initial impurity-produced H atom concentrations of less than approximately 0.02 ppm for our test conditions. In addition, no laser absorption was noted in shock-heated pure Ar, $H_2$/Ar, and $O_2$/Ar mixtures.

The uncertainty in $k_2$ due to uncertainties in temperature, pressure, and secondary reaction rates was estimated by individually perturbing each parameter by its estimated uncertainty and adjusting $k_2$ to regain a best fit of the OH profile. An overall uncertainty of approximately ±10% is estimated by assuming the individual uncertainties are independent and taking the square root of the sum of the squares of the individual uncertainty contributions. The primary contributors are the ±4% scatter in the rate data, sensitivity to all secondary reactions (less than ±5% total), determination of best fit (typically ±3%), ±0.4% temperature uncertainty (resulting in an approximate ±1–2% uncertainty in $k_2$), discrepancies between calculated and observed OH plateaus, and the above vibrational relaxation and boundary layer development considerations. The uncertainty in the highest temperature data point at $T$ = 3370 K is larger, an estimated ±18%, primarily due to the uncertainty in $k_{17}$ and its increased contribution to the radical pool.

## Discussion

The present determination of $k_2$ from OH absorption measurements is compared to other recent studies in Figure 7. The present determination falls between the CO–O flame-band emission results of Schott[2] and the more recent combined O atom and H atom ARAS results of Frank and Just,[5] which are in close agreement with the earlier recommendation of Baulch.[1] The Schott determination has long been questioned due to a stated negative temperature curvature ($T^{-0.907}$) which effectively gives an activation energy less than the endothermicity. The accuracy of the Schott determinations at high temperature has also been questioned due to the assumption of exponential growth of radical concentrations at high temperatures.[33] Trajectory calculations of Miller[10,11] argue in favor of the negative temperature dependence of the Schott rate coefficient due to "nonstatistical recrossing" of the transition state dividing surfaces at high temperature. The results of the Miller calculations,[11] also plotted in Figure 7, are in close agreement with the Schott determination. However, the theoretical calculations of the reverse reaction by Troe[12] are closer to agreement with the $k_2$ values of Frank and Just,[5] but with a significantly lower activation energy for the forward rate (15.5 kcal mol$^{-1}$). The recent studies of Pamidimukkala and Skinner,[4] Frank and Just,[5] Vandooren et al.,[7] and Pirraglia et al.[8] reported Arrhenius expressions with activation energies of 16.1 (1000–2500 K), 17.3 (1700–2500 K), 14.7 (1000–1350 K), and 16.1 kcal mol$^{-1}$ (962–1705 K), respectively. The two studies of Fujii et al.[6,46] report very large activation energies of 22.7 (1900–2650 K) and 20.6 kcal mol$^{-1}$ (1700–2700 K), as determined with OH laser absorption and O atom ARAS, respectively.

Over the 1700–2500 K temperature range of the Frank and Just[5] study, the present rate determination is 21–38% lower, and it is 6–32% higher than Schott[1] in the 1450–2500 K temperature overlap. The H atom and O atom ARAS measurements of Frank and Just are sensitive to the choice of the rates of reactions 1 and 3. Fitting the high-temperature O atom trace presented in their publication (at $T$ = 2368 K) with the rates for reactions 1 and 3 used here would result in a rate for reaction 2 approximately 20% higher than ours, which is within the combined uncertainties of our work and theirs. This would also lower their activation energy by approximately 2 kcal mol$^{-1}$. Conversely, substitution of their chosen rate coefficients for reactions 1 and 3 into our mechanism would have less than a 3% effect on the present rate determination.

Yuan et al.[9] recently reported a rate coefficient determination over the temperature range 1050–2700 K which is in close agreement with that of Schott. They also used OH laser absorption in $H_2/O_2$/Ar mixtures with $H_2$:$O_2$ ratios varying from very lean (1:9) to moderately rich (4:1). Although the reported fit of their data falls from 3% to 23% below the fit of the present

(40) Kiefer, J. H.; Lutz, R. W. *J. Chem. Phys.* **1966**, *44*, 668.
(41) Rao, V. S.; Skinner, G. B. *J. Chem. Phys.* **1984**, *81*, 775.
(42) Zuhrt, Ch.; Zulicke, L.; Umansky, S. Ya. *Chem. Phys.* **1986**, *105*, 15.
(43) Zellner, R. In *Combustion Chemistry*; Gardiner, Jr., W. C., Ed.; Springer-Verlag: New York, 1984; Chapter 4.
(44) Brown, R. C. *Combust. Flame* **1985**, *62*, 1.
(45) Birely, J. H.; Lyman, J. L. *J. Photochem.* **1975**, *4*, 269.
(46) Fujii, N.; Sato, T.; Miyama, H.; Shin, K.; Gardiner, W. C. *Seventeenth Symposium (International) on Shock Tubes and Waves*, to be published.

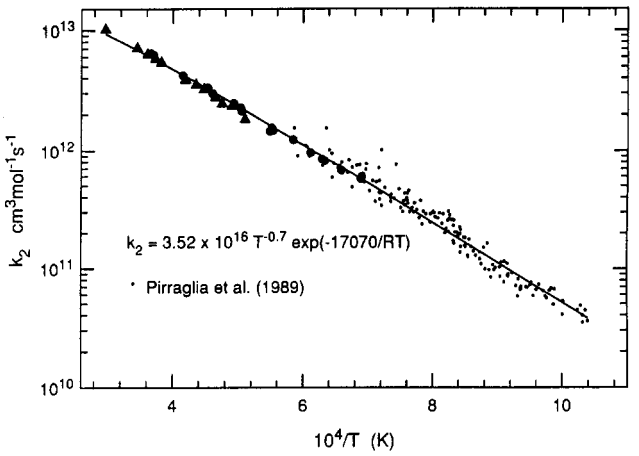


**Figure 11.** Arrhenius plot of rate coefficients for reaction 2, H + $O_2$ → OH + O: circles, incident shock data; triangles, reflected shock data; solid line, three-parameter fit to the combined data of Pirraglia et al.[8] and the present OH absorption data.

measurements over the temperature range 1450–2700 K, the determinations are in agreement within the approximately 30% and 10% uncertainties of their and our respective rate determinations. The systematic difference is at least partially due to their choice of a higher rate for the initiation reaction 7 to which they are sensitive. The large uncertainty in the initiation reaction rate coefficient also contributes to their larger $k_2$ determination uncertainty.

The rate coefficient data derived from the OH laser absorption measurements of Fujii and Shin[6] are marginally within combined uncertainties over the entire temperature range of their measurements, although in different directions at the temperature extremes resulting in a very high activation energy. We are unable to explain the strong temperature dependence they observed.

Pirraglia et al.[8] determined $k_2$ using ARAS to monitor H atom production in flash-photolyzed mixtures of $NH_3/O_2/Ar$ and $H_2O/O_2/Ar$ in shock tube experiments in the 926–1705 K temperature range. The present rate coefficient expression yields $k_2$ values 10–20% lower than those obtained from the reported fit of the ARAS data in the 1450–1705 K temperature overlap; however, the two data sets agree to well within the combined scatter. The experimental data set of Pirraglia et al. are combined with the present data for $k_2$ in Figure 11. The difference in the respective activation energies suggests that the combined sets are best fit with three variable parameters. A least-squares three-parameter fit over the temperature range 962–3370 K was determined to be

$$k_2 = 3.52 \times 10^{16} T^{-0.7} \exp(-17070 \text{ cal mol}^{-1}/RT, \text{ K}) \quad \text{cm}^3 \text{ mol}^{-1} \text{ s}^{-1}$$

The preexponential temperature dependence, $b = -0.7$, is close to that determined by Schott[2] ($b = -0.907$) and calculated by Miller[10] ($b = -0.816$).

The present determinations of $k_2$ from H atom ARAS measurements (Figure 10) are compared with the rates determined by Pamidimukkala and Skinner[4] and by Fujii et al.,[46] both from O atom ARAS measurements in reflected shock-heated $H_2/O_2/Ar$ mixtures. Agreement among these studies is considered good although again the activation energy of Fujii et al. appears to be high. The previously discussed simultaneous H atom and O atom ARAS determination of $k_2$ by Frank and Just[5] is also shown.

The reverse rate $k_{-2}$ was calculated for each of our rich mixture data points in Figure 7 by using equilibrium constants from the Sandia National Laboratories thermodynamic data base;[31] the results are plotted in Figure 12. Our data alone do not extend over a sufficiently wide temperature range to exhibit significant temperature dependence for the reverse reaction. A least-squares fit of our data combined with the low-temperature data of Howard and Smith[47] to the form $aT^b$ gives

$$k_{-2} = 2.02 \times 10^{14} T^{-0.40(\pm 0.02)} \quad \text{cm}^3 \text{ mol}^{-1} \text{ s}^{-1}$$

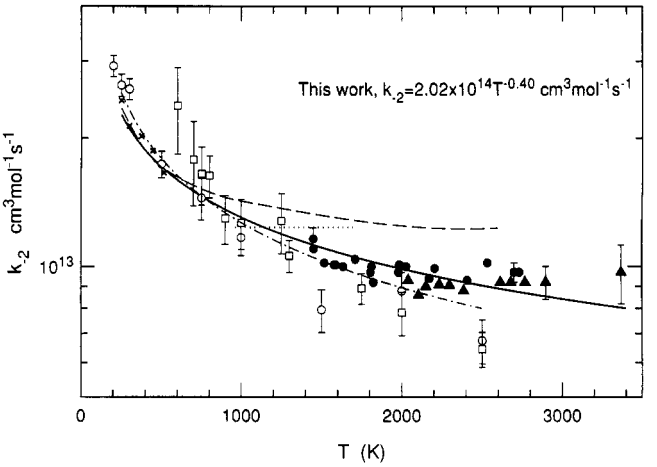


**Figure 12.** Rate coefficients for the reverse reaction O + OH → H + $O_2$ determined from rich mixture OH absorption experiments and the equilibrium constant: solid circles, incident shock data; triangles, reflected shock data; ×, Howard and Smith;[47] open circles, Miller QCT calculation of $k_{-2}$,[11] open squares, $k_{-2}$ from Miller QCT calculation of $k_2$ and the equilibrium constant; solid line, least-squares fit to the combined data of Howard and Smith[47] and the present OH absorption data; dotted line, result of Pirraglia et al.;[8] dashed line, calculation of Troe;[12] dot-dash line, expression of Howard and Smith[47] extended to 2500 K as recommended by Miller.[11]

This expression lies between the theoretical calculations of Miller[11] and Troe[12] with a negative temperature dependence, $b = -0.40$, which is slightly lower than the $b = -0.50$ recommended by Miller[11] for the temperature range 200–2500 K. The results of trajectory calculations and recommended expression of Miller[11] are also plotted. Agreement with the present results is within approximately 10% up to 2500 K.

## Conclusions

The rate coefficient of the chain-branching reaction H + $O_2$ → OH + O was determined by using OH laser absorption over the temperature range 1450–3370 K in combined incident and reflected shock wave experiments. The resulting least-squares fit

$$k_2 = (9.33 \pm 0.40) \times 10^{13} \exp\{-(14800 \pm 170) \text{ cal mol}^{-1}/RT, \text{ K}\} \quad \text{cm}^3 \text{ mol}^{-1} \text{ s}^{-1}$$

lies below the determination of Frank and Just[5] and Baulch recommendation[1] but above the long-used rate expression of Schott[2] and the recent results of a similar OH laser absorption study by Yuan et al.[9] However, agreement with Yuan is within the combined uncertainties of the two experiments. Although no preexponential temperature dependence is apparent from our data, combination with the recent determination of Pirraglia et al.[8] results in a best-fit expression of

$$k_2 = 3.52 \times 10^{16} T^{-0.7} \exp(-17070 \text{ cal mol}^{-1}/RT, \text{ K}) \quad \text{cm}^3 \text{ mol}^{-1} \text{ s}^{-1}$$

with a negative preexponential temperature dependence similar to although smaller than calculated by Miller[10] and determined experimentally by Schott.[2] Combination of the present data with the low-temperature reverse reaction rate determinations of Howard and Smith[47] further supports a negative temperature preexponential dependence. It should be noted that both the

(47) Howard, M. J.; Smith, I. W. M. *J. Chem. Soc., Faraday Trans. 2* **1981**, *77*, 997.
(48) Sutherland, J. W.; Michael, J. V.; Pirraglia, A. N.; Nesbitt, F. L.; Klemm, R. B. *Twenty-First Symposium (International) on Combustion*; The Combustion Institute: Pittsburgh, 1988; p 929.
(49) Miller, J. A.; Bowman, C. T. *Prog. Energy Combust. Sci.* **1989**, *15*, 287.
(50) Troe, J. *Ber. Bunsen-Ges. Phys. Chem.* **1969**, *73*, 946.
(51) Hanson, R. K.; Salimian, S. In *Combustion Chemistry*; Gardiner, Jr., W. C., Ed.; Springer-Verlag: New York, 1984; Chapter 6.

scatter and the estimated uncertainty of our results are improved relative to previous work.

*Acknowledgment.* This work was supported by the U.S. Department of Energy, Office of Basic Energy Sciences, Division of Chemical Sciences. We thank Albert Y. Chang and Michael D. DiRosa for assistance in the laboratory and David F. Davidson and James A. Miller for helpful discussions.

**Registry No.** H, 12385-13-6; $O_2$, 7782-44-7.

# Picosecond Raman Investigation of Interligand Electron Transfer in Ruthenium(II) Complexes

**T. Yabe, L. K. Orman, D. R. Anderson, Soo-Chang Yu, Xiaobing Xu, and J. B. Hopkins***

*Department of Chemistry, Louisiana State University, Baton Rouge, Louisiana 70803*
*(Received: January 16, 1990; In Final Form: May 9, 1990)*

Interligand electron transfer has been investigated in the excited MLCT electronic states of mixed ligand ruthenium(II) polypyridine complexes containing bipyridine, bipyrimidine, and carboxybipyridine. Two-color picosecond Raman spectroscopy has been used to unambiguously establish the vibrational spectrum corresponding to the ligand-localized MLCT states. With these data direct measurements of electron-transfer dynamics are obtained. It is found that interligand electron transfer is complete on a time scale significantly faster than the 30-ps experimental time resolution.

## Introduction

The photochemistry of Ru(II) complexes has been extensively studied and is still of wide interest[1] since the complexes represent a potential source of electrons that can be pumped into subsequent reactions. The excited triplet MLCT states have been characterized as having the photoexcited electron localized on one ligand.[2-4] In recent years, there has been great interest in understanding the rate of interligand electron transfer (ILET) following MLCT excitation. By characterization of the rates of ILET, it should be possible to determine the mechanisms leading to electron localization on the excited-state potential surface. In addition, since these molecules have a fixed distance between the electron donor and acceptor ligands, they provide excellent models to test the effects of electronic coupling and energy gap on rates of electron transfer (ET).

There have been many recent attempts to measure interligand ET rates, using various time-resolved techniques. Dual emitting states have been observed in complexes of Rb[5] and Ir.[6] For Ru(II) the emission spectrum in mixed-ligand complexes is found to be nearly identical from each chromophore. As a result, time-resolved measurements of electron transfer are virtually impossible. In addition, the electronic coupling in Ru(II) complexes is thought to be much higher than for other metals. Due to this fact, ET rates are expected to be higher in complexes containing Ru(II).[7] It has recently become possible to directly measure ILET by utilization of time-resolved Raman techniques.[8-10] With this method, detailed information pertaining to ligand-specific molecular structure can be obtained by means of vibrational frequencies.

This paper discusses the use of picosecond Raman spectroscopy to measure ILET in mixed-ligand complexes of 2,2′-bipyridine (bpy) with 2,2′-bipyrimidine (bpym) or 4,4′-dicarboxy-2,2′-bipyridine (carboxy-bpy). Two-color Raman spectroscopy is used to increase the confidence of the spectroscopic assignments. In addition, this method significantly reduces the spectral congestion by removing ground-state bands from the spectrum. Conclusions regarding ILET dynamics are therefore much more straightforward. These results provide an excellent opportunity to investigate the relative importance of electronic coupling and nuclear tunneling to electron-transfer processes.

* Author to whom correspondence should be addressed.

## Experimental Section

The experimental apparatus has been previously described in detail.[8-10] The picosecond laser is based on a high repetition rate (2 kHz) regenerative laser[11,12] that amplifies chirped pulses from a Quantronix 416 mode-locked laser. Following temporal compression, the laser pulses have a 30-ps pulse width and 1.25 mJ of energy at 1.064 μm. Harmonic generation in BBO (β-barium borate) converts the fundamental laser frequency to the second and third harmonics used in this experiment. One-color excitation takes place in a rotating cell to ensure that no two pulses interrogate the same region of sample. In the two-color experiments both a free flowing jet and flowing quartz cell were used. Triply distilled water was used as the solvent in all aspects of this work. A conventional scanning double monochromator is used as the dispersive apparatus. Detection consists of a photomultiplier tube and gated integration.

The two-color experiment has been previously described in detail.[8-10] Chopped laser excitation (100 Hz) is used to rapidly obtain raw two-color and one-color background spectra in a single scan of the monochromator. The transient spectrum is computed

(1) (a) Nocera, D. G.; Winkler, J. R.; Yocom, K. M.; Bordignon, E.; Gray, H. B. *J. Am. Chem. Soc.* **1984**, *106*, 5145. (b) Krueger, J. S.; Mayer, J. E.; Mallouk, T. E. *J. Am. Chem. Soc.* **1988**, *100*, 8232.
(2) (a) Bradley, P. B.; Hornberger, B. A.; Dallinger, R. F.; Woodruff, W. H. *J. Am. Chem. Soc.* **1981**, *103*, 7441. (b) Casper, J. V.; Westmoreland, T. D.; Allen, G. H.; Bradley, P. B.; Meyer, T. J.; Woodruff W. H. *J. Am. Chem. Soc.* **1984**, *106*, 3492.
(3) Carlin, C. M.; DeArmond, M. K. *Chem. Phys. Lett.* **1982**, *89*(4), 297.
(4) Carroll, P. J.; Brus, L. E. *J. Am. Chem. Soc.* **1987**, *109*, 7613.
(5) Halper, W.; DeArmond, M. K. *J. Lumin.* **1972**, *5*, 225.
(6) (a) Watts, R. J.; Brown, M. J.; Griffith, B. G.; Harrington, J. S. *J. Am. Chem. Soc.* **1975**, *97*, 6029. (b) Watts, R. J.; Griffith, B. G.; Harrington, J. S. *J. Am. Chem. Soc.* **1976**, *98*, 674. (c) Watts, R. J.; White, T. P.; Griffith, B. G. *J. Am. Chem. Soc.* **1975**, *97*, 6914.
(7) DeArmond, M. K.; Carlin, C. M. *Coord. Chem. Rev.* **1981**, *36*, 325.
(8) Orman, L. K.; Hopkins, J. B. *Chem. Phys. Lett.* **1988**, *149*, 375.
(9) Orman, L. K.; Chang, Y. J.; Anderson, D. R.; Yabe, T.; Xu, Xiaobing; Yu, Soo-Chang; Hopkins, J. B. *J. Chem. Phys.* **1989**, *90*, 1469.
(10) Chang, Y. J.; Xu, Xiaobing; Yabe, T.; Yu, Soo-Chang; Anderson, D. R.; Orman, L. K.; Hopkins, J. B. *J. Phys. Chem.*, in press.
(11) Chang, Y. J.; Veas, C.; Hopkins, J. B. *Appl. Phys. Lett.* **1986**, *49*, 1758.
(12) Chang, Y. J.; Anderson, D. R.; Hopkins, J. B. *International Conference on Lasers; 1986*; McMillan, R. W.; Ed.; STS Press: McLean, VA, 1987; p 169.

0022-3654/90/2094-7128$02.50/0 